Supplementary material

Tables

Table S1. Manuscripts from which bulk rock and serpentine specific Fe chemical and redox data was obtained. Asteriks indicate manuscripts included in bulk rock FeIII/Fe_T vs. H_2O wt% plot presented in Evans 2008.

Table S2. Statistics for bulk rock Fe chemistry of serpentinites grouped by rock type, sample type, and measurement method.

Table S3. Statistics for serpentine mineral Fe chemistry grouped by rock type, sample type, and measurement method.

(Tables S2 and S3 include data from all categories regardless of the number of specimens in each category.)

Figure Captions

Figure S1. Histograms of bulk rock Fe chemistry of serpentinites. A) Total FeO abundance (wt%) by rock type. B) Total FeO wt% by sample type. C) Total FeO wt% by analytical method. D) Total FeIII abundance (wt%) by rock type. E) Total FeIII wt% by sample type. F) Total FeIII wt% by analytical method. G) FeIII/Fe_T by rock type. H) FeIII/Fe_T by sample type. I) FeIII/Fe_T by analytical method. Diamonds indicate mean values and filled circles indicate median values. F statistic and p-value results of ANOVA tests are shown at the top of each plot. Letters represent the results of pairwise comparison tests where each letter represents a statistically significantly different category. Categories sharing common letters are not statistically significantly different from one another.

Figure S2. Histograms of bulk rock Fe chemistry of serpentinites by geologic setting as described by the original source of the data (plots A, C, E) and inferred initial setting/process (plots (B, D, F). A and B) Total FeO abundance (wt%). C and D) Total FeIII abundance (wt%). E and F) FeIII/Fe_T. Diamonds indicate mean values and filled circles indicate median values. F statistic and p-value results of ANOVA tests are shown at the top of each plot. Letters represent the results of pairwise comparison tests where each letter represents a statistically significantly different category. Categories sharing common letters are not statistically significantly different from one another.

Figure S3. Bulk rock total FeO content as a function of the extent of serpentinization using LOI wt% as a proxy for extent of serpentinization. This data includes carbonated serpentinites that have LOI values up to ~50 wt%, much greater than typical serpentinites (max LOI ~15 wt%).

Figure S4. Histograms of the Fe chemistry of serpentine minerals. A) Total FeO abundance (wt%) by rock type. B) Total FeO wt% by sample type. C) Total FeIII abundance (wt%) by sample type. D) FeIII/Fe_T by sample type. E) FeIII/Fe_T by analytical method. Diamonds indicate mean values and filled circles indicate median values. F statistic and p-value results of ANOVA tests are shown at the top of each plot. Letters represent the results of pairwise

comparison tests where each letter represents a statistically significantly different category. Categories sharing common letters are not statistically significantly different from one another.

Figure S5. Histograms of Fe chemistry of serpentine minrerals by geologic setting as described by the original source of the data (plots A, C, E) and inferred initial setting/process (plots (B, D, F). A and B) Total FeO abundance (wt%). C and D) Total FeIII abundance (wt%). E and F) $FeIII/Fe_T$. Diamonds indicate mean values and filled circles indicate median values. F statistic and p-value results of ANOVA tests are shown at the top of each plot. Letters represent the results of pairwise comparison tests where each letter represents a statistically significantly different category. Categories sharing common letters are not statistically significantly different from one another.

Figure S6. A) Total FeO abundance (wt%) of serpentine versus bulk rock total FeO abundance (wt%). B) Total FeO wt% versus bulk rock LOI wt% as a proxy for extent of serpentinization.

Table S1.

Agrinier P., Hekinian R., Bideau D. and Javoy M. (1995) O and H stable isotope compositions of oceanic crust and upper mantle rocks exposed in the Hess Deep near the Galapagos Triple Junction. *Earth and Planetary Science Letters* **136**, 183–196.

Agrinier P. and Cannat M. (1997) Oxygen-isotope constraints on serpentinization processes in ultramafic rocks from the mid-Atlantic Ridge (23N) eds. J. A. Karson, M. Cannat, D. J. Miller, and D. Elthon. Proceedings of the Ocean Drilling Program Results 153.

Andreani M., Escartin J., Delacour A., Ildefonse B., Godard M., Dyment J., Fallick A. E. and Fouquet Y. (2014) Tectonic structure, lithology, and hydrothermal signature of the Rainbow massif (Mid-Atlantic Ridge 36°14′N). *Geochemistry, Geophysics, Geosystems* **15**, 3543–3571.

Andreani M., Muñoz M., Marcaillou C. and Delacour A. (2013) µXANES study of iron redox state in serpentine during oceanic serpentinization. *Lithos* **178**, 70–83.

*Anselmi B., Mellini M. and Viti C. (2000) Chlorine in the Elba, Monti Livornesi and Murlo serpentines: evidence for sea-water interaction. *European Journal of Mineralogy* **12**, 137–146.

Augustin N., Lackschewitz K. S., Kuhn T. and Devey C. W. (2008) Mineralogical and chemical mass changes in mafic and ultramafic rocks from the Logatchev hydrothermal field (MAR 15°N). *Marine Geology* **256**, 18–29.

*Aumento F. and Loubat H. (1971) The Mid-Atlantic Ridge Near 45 °N. XVI. Serpentinized Ultramafic Intrusions. *Can. J. Earth Sci.* **8**, 631–663.

*Bertrand J., Courtin B. and Vuagnat M. (1982) Elaboration d'un secteur de lithosphère océanique liguro-piemontais d'apres les données de l'ophiolite du Montgenèvre (Hautes-Alpes, France et province de Turin, Italie). *Ofioliti* **7**, 155–196.

*Bertrand and Vuagnat (1980) Inclusions in the serpentinite melange of the Motagua Fault Zone, Guatemala. *Archives des Science Genève* **33**, 321–336.

Blaauw C., Stroink G., Leiper W. and Zentilli M. (1979) Mossbauer analysis of some Canadian chrysotiles. *Canadian Mineralogist* **17**, 713–717.

Bodinier J. L. (1988) Geochemistry and petrogenesis of the Lanzo peridotite body, western Alps. *Tectonophysics* **149**, 67–88.

*Bonatti E. (1968) Ultramafic Rocks from the Mid-Atlantic Ridge. *Nature* **219**, 363–364.
Bonnemains D., Carlut J., Escartín J., Mével C., Andreani M. and Debret B. (2016) Magnetic signatures of serpentinization at ophiolite complexes: magnetism of ophiolite serpentinites. *Geochemistry, Geophysics, Geosystems* **17**, 2969–2986.

Boschi C., Früh-Green G. L., Delacour A., Karson J. A. and Kelley D. S. (2006) Mass transfer and fluid flow during detachment faulting and development of an oceanic core complex, Atlantis Massif (MAR 30°N): mass transfer and fluid flow. *Geochemistry, Geophysics, Geosystems* **7**.

Bowin C. O., Nalwalk A. J. and Hersey J. B. (1966) Serpentinized Peridotite from the North Wall of the Puerto Rico Trench. *Geological Society of America Bulletin* **77**, 257.

*Brunacci S., Faraone D. and Giaquinto S. (1976) Indagini petrografiche e chimiche su ofioliti della Toscana. 2-Gli afioramenti nei dintorni di Pieve S. Stefano (Arezzo). *Ofioliti* **1**, 163–193.

*Coleman R. G. and Keith T. E. (1971) A Chemical Study of Serpentinization--Burro Mountain, California. *Journal of Petrology* **12**, 311–328.

D'Antonio M. and Kristensen M. B. (2004) Serpentine and brucite of ultramafic clasts from the South Chamorro Seamount (Ocean Drilling Program Leg 195, Site 1200): inferences for the serpentinization of the Mariana forearc mantle. *Mineralogical Magazine* **68**, 887–904.

Debret B., Andreani M., Muñoz M., Bolfan-Casanova N., Carlut J., Nicollet C., Schwartz S. and Trcera N. (2014) Evolution of Fe redox state in serpentine during subduction. *Earth and Planetary Science Letters* **400**, 206–218.

Debret B., Bolfan-Casanova N., Padrón-Navarta J. A., Martin-Hernandez F., Andreani M., Garrido C. J., López Sánchez-Vizcaíno V., Gómez-Pugnaire M. T., Muñoz M. and Trcera N. (2015) Redox state of iron during high-pressure serpentinite dehydration. Contributions to Mineralogy and Petrology 169.

Delacour A., Früh-Green G. L., Frank M., Gutjahr M. and Kelley D. S. (2008) Sr- and Nd-isotope geochemistry of the Atlantis Massif (30°N, MAR): Implications for fluid fluxes and lithospheric heterogeneity. *Chemical Geology* **254**, 19–35.

Engin T. and Hirst D. M. (1970) Serpentinisation of harzburgites from the alpine peridotite belt of Southwest Turkey. *Chemical Geology* **6**, 281–295.

Evans B. W., Dyar M. D. and Kuehner S. M. (2012) Implications of ferrous and ferric iron in antigorite. *American Mineralogist* **97**, 184–196.

Evans B. W., Kuehner S. M. and Chopelas A. (2009) Magnetite-free, yellow lizardite serpentinization of olivine websterite, Canyon Mountain complex, N.E. Oregon. *American Mineralogist* **94**, 1731–1734.

Evans K. A. (2012) The redox budget of subduction zones. *Earth-Science Reviews* **113**, 11–32.

Evans K. A., Reddy S. M., Tomkins A. G., Crossley R. J. and Frost B. R. (2017) Effects of geodynamic setting on the redox state of fluids released by subducted mantle lithosphere. *Lithos* **278**–**281**, 26–42.

Fruh-Green G., Plas A. and Lecuyer C. (1996) Petrologic and stable isotope constraints on hydrothermal alteration and serpentinization of the EPR shallow mantle at Hess Deep (site 895). *Proceedings of the Ocean Drilling Program, Scientific Results* **147**, 255–288.

Fuchs Y., Linares J. and Mellini M. (1998) Mössbauer and infrared spectrometry of lizardite-1T from Monte Fico, Elba. *Phys Chem Min* **26**, 111–115.

Godard M., Awaji S., Hansen H., Hellebrand E., Brunelli D., Johnson K., Yamasaki T., Maeda J., Abratis M., Christie D., Kato Y., Mariet C. and Rosner M. (2009) Geochemistry of a long in-situ section of intrusive slow-spread oceanic lithosphere: Results from IODP Site U1309 (Atlantis Massif, 30°N Mid-Atlantic-Ridge). *Earth and Planetary Science Letters* **279**, 110–122.

Godard M., Jousselin D. and Bodinier J.-L. (2000) Relationships between geochemistry and structure beneath a palaeo-spreading centre: a study of the mantle section in the Oman ophiolite. *Earth and Planetary Science Letters* **180**, 133–148.
*Green D. H. (1964) The petrogenesis of the high-temperature peridotite intrusion. In *in the Lizard Area* pp. 134–188.

*Grubb P. L. C. (1962) Serpentinization and chrysotile formation in the Matheson ultrabasic belt, northern Ontario. *Economic Geology* **57**, 1228–1246.

Hanghoj K., Kelemen P. B., Hassler D. and Godard M. (2010) Composition and Genesis of Depleted Mantle Peridotites from the Wadi Tayin Massif, Oman Ophiolite; Major and Trace Element Geochemistry, and Os Isotope and PGE Systematics. *Journal of Petrology* **51**, 201–227.

*Hatzlpanagiotou K. Petrography of the ophiolite complex in central argolis (peloponnesus, greece). **15**:61-67.

*Hébert R., Serri G. and Hékinian R. (1989) Mineral chemistry of ultramafic tectonites and ultramafic to gabbroic cumulates from the major oceanic basins and Northern Apennine ophiolites (Italy) — A comparison. *Chemical Geology* **77**, 183–207.

*Hess H. H. (1964) The oceanic crust, the upper mantle, and the Mayaguez serpentinized peridotite. In *A study of serpentinite the AMSOC core hole near Mayaguez, Puerto Rico* pp. 169–175.

*Hess H. H. and Otalora G. (1964) Mineralogical and chemical composition of the Mayaguez Serpentinite cores. In *A study of serpentinite the AMSOC core hole near Mayaguez, Puerto Rico* pp. 152–168.

*Ishii T., Robinson P. T., Maekawa H. and Fiske R. (1992) 27. Petrological studies of the peridotites from diapiric serpentinite seamounts in the Izu-Ogasawara-Mariana forearc, Leg 125. *Proceedings of the Ocean Drilling Program, Scientific Results* **125**, 445–485.

*Ivanov T., Misar Z., Bowes D. and Dudek A. (1987) The Demir Kapija-Gevgelija ophiolite massif, Macedonia, Yugoslavia. *Ofioliti* **12**, 457–478.

*Joplin G. A. (1963) *Chemical analyses of Australian Rocks. Part I: Igneous and metamorphic*., Bureau of Mineral Resources, Geology and Geophysics.

Kahl W.-A., Jöns N., Bach W., Klein F. and Alt J. C. (2015) Ultramafic clasts from the South Chamorro serpentine mud volcano reveal a polyphase serpentinization history of the Mariana forearc mantle. *Lithos* **227**, 1–20.

Klein F., Bach W., Humphris S. E., Kahl W.-A., Jons N., Moskowitz B. and Berquo T. S. (2014) Magnetite in seafloor serpentinite--Some like it hot. *Geology* **42**, 135–138.

Klein F., Bach W., Jöns N., McCollom T., Moskowitz B. and Berquó T. (2009) Iron partitioning and hydrogen generation during serpentinization of abyssal peridotites from 15°N on the Mid-Atlantic Ridge. *Geochimica et Cosmochimica Acta* **73**, 6868–6893.
Kodolányi J., Pettke T., Spandler C., Kamber B. S. and Gméling K. (2012) Geochemistry of Ocean Floor and Fore-arc Serpentinites: Constraints on the Ultramafic Input to Subduction Zones. *J Petrology* **53**, 235–270.

*Koepke J., Kreuzer H. and Seidel E. (1985) Ophiolites in the southern Aegean Arc (Crete, Karpathos, Rhodes)–linking the ophiolite belts of the Hellenides and the Taurides. *Ofioliti* **10**, 343–354.

*Laurent R. (1975) Petrology of the alpine-type serpentinites of asbestos and Thetford Mines, Quebec. *Schweizerische mineralogische und petrographische Mitteilungen = Bulletin suisse de minéralogie et pétrographie* **55**, 431–455.

*Livingstone A. (1976) A metamorphosed, layered alpine-type peridotite in the Langavat Valley, South Harris, Outer Hebrides. *Mineralogical Magazine* **40**, 493–499.

*Loney R. A., Himmelberg G. R. and Coleman R. G. (1971) Structure and Petrology of the Alpine-type Peridotite at Burro Mountain, California, U.S.A. *Journal of Petrology* **12**, 245–309.

Mayhew L. E., Ellison E. T., Miller H. M., Kelemen P. B. and Templeton A. S. (2018) Iron transformations during low temperature alteration of variably serpentinized rocks from the Samail ophiolite, Oman. *Geochimica et Cosmochimica Acta* **222**, 704–728.

Miller H. M., Matter J. M., Kelemen P., Ellison E. T., Conrad M. E., Fierer N., Ruchala T., Tominaga M. and Templeton A. S. (2016) Modern water/rock reactions in Oman hyperalkaline peridotite aquifers and implications for microbial habitability. *Geochimica et Cosmochimica Acta* **179**, 217–241.

*Milliken K. L., Lynch F. L. and Seifert K. E. (1996) 31. Marine weathering of serpentinites and serpentinite breccias, Sites 897 and 899, Iberia Abyssal Plain. *Proceedings of the Ocean Drilling Program, Scientific Results* **149**, 529–540.

*Miyashiro A., Shido F. and Ewing M. (1969) Composition and origin of serpentinites from the Mid-Atlantic Ridge near 24° and 30° North Latitude. *Contr. Mineral. and Petrol.* **23**, 117–127.

Mothersole F. E., Evans K. and Frost B. R. (2017) Abyssal and hydrated mantle wedge serpentinised peridotites: a comparison of the 15∘20′N fracture zone and New Caledonia serpentinites. *Contrib Mineral Petrol* **172**, 69.

*Mumpton F. A. (1975) Mineralogy and Origin of the Coalinga Asbestos Deposit. *Clays and Clay Minerals* **23**, 131–143.

O'Hanley D.S. and Dyar M. D. (1993) The composition of lizardite 1T and the formation of magnetite in serpentinites. **78**:391-404.

O'Hanley D. S. and Dyar M. D. (1998) The composition of chrysotile and its relationship with lizardite. *The Canadian Mineralogist*, 36:727-739.

*O'Hanley D. S. and Offler R. (1992) Characterizatio of multiple serpentinization, Woodsreef, New South Wales. *The Canadian Mineralogist*, **30**, 1113–1126.

*O'Hanley D. S. and Wicks F. J. (1995) Conditions of formation of lizardite, chrysotile and antigorite, Cassiar, British Columbia. *The Canadian Mineralogist* **33**, 753–773.

Oufi O. (2002) Magnetic properties of variably serpentinized abyssal peridotites. Journal of Geophysical Research 107.

Padrón-Navarta J. A., López Sánchez-Vizcaíno V., Garrido C. J. and Gómez-Pugnaire M. T. (2011) Metamorphic Record of High-pressure Dehydration of Antigorite Serpentinite to Chlorite Harzburgite in a Subduction Setting (Cerro del Almirez, Nevado–Filábride Complex, Southern Spain). *J Petrology* **52**, 2047–2078.

Paulick H., Bach W., Godard M., De Hoog J. C. M., Suhr G. and Harvey J. (2006) Geochemistry of abyssal peridotites (Mid-Atlantic Ridge, 15°20′N, ODP Leg 209): Implications for fluid/rock interaction in slow spreading environments. *Chemical Geology* **234**, 179–210.

Roumejon S., Cannat M., Agrinier P., Godard M. and Andreani M. (2015) Serpentinization and Fluid Pathways in Tectonically Exhumed Peridotites from the Southwest Indian Ridge (62-65 E). *Journal of Petrology* **56**, 703–734.

Rouméjon S., Früh-Green G. L. and Orcutt B. N. (2018a) Alteration Heterogeneities in Peridotites Exhumed on the Southern Wall of the Atlantis Massif (IODP Expedition 357). *J Petrology* **59**, 1329–1358.

Rouméjon S., Williams M. J. and Früh-Green G. L. (2018b) In-situ oxygen isotope analyses in serpentine minerals: Constraints on serpentinization during tectonic exhumation at slow- and ultraslow-spreading ridges. *Lithos* **323**, 156–173.

*Rumori C., Mellini M. and Viti C. (2004) Oriented, non-topotactic olivine → serpentine replacement in mesh-textured, serpentinized peridotites. *European Journal of Mineralogy* **16**, 731–741.

*Savu H., Udrescu C., Neacsu V., Bratosin I. and Stoian M. (1985) Origin, geochemistry and tectonic position of the Alpine ophiolites in the Severin Nappe (Mehedinti Plateau, Romania). *Ofioliti* **10**, 423–440.

*Seifert K. and Brunotte D. (1996) 23. Geochemistry of serpentinized mantle peridotite from Site 897 in the Iberia Abyssal Plain. *Proceedings of the Ocean Drilling Program, Scientific Results* **149**, 413–424.
Streit E., Kelemen P. and Eiler J. (2012) Coexisting serpentine and quartz from carbonate-bearing serpentinized peridotite in the Samail Ophiolite, Oman. *Contributions to Mineralogy and Petrology* **164**, 821–837.

*Trommsdorff V. and Evans B. W. (1972) Progressive metamorphism of antigorite schist in the Bergell tonalite aureole (Italy). *Am J Sci* **272**, 423–437.

*Van Calsteren P. W. C. (1978) Geochemistry of the polymetamorphic mafic-ultramafic complex at Cabo Ortegal (NW Spain). *Lithos* **11**, 61–72.

*Viti C. and Mellini M. (1998) Mesh textures and bastites in the Elba retrograde serpentinites. *European Journal of Mineralogy* **10**, 1341–1360.

*Weber-Diefenbach K., Davoudzadeh M. and Alavi-Tehrani N. (1986) Paleozoic ophiolites in Iran. Geology, Geochemistry and geodynamic implication. *Ofioliti* **11**, 305–338.

Wicks F. J. and Plant A. G. (1979) electron-microprobe and x-ray-microbeam studies of serpentine textures. *The Canadian Mineralogist* **17**, 785-830.

Zega T. J., Garvie L. A. J. and Buseck P. R. (2003) Nanometer-scale measurements of iron oxidation states of cronstedtite from primitive meteorites. *American Mineralogist* **88**, 1169–1172.

Zega T. J., Garvie L. A. J., Dódony I. and Buseck P. R. (2004) Serpentine nanotubes in the Mighei CM chondrite. *Earth and Planetary Science Letters* **223**, 141–146.

Zega T. J., Garvie L. A. J., Dódony I., Friedrich H., Stroud R. M. and Buseck P. R. (2006) Polyhedral serpentine grains in CM chondrites. *Meteoritics & Planetary Science* **41**, 681–688.

Table S2.

	FeO_T (wt%)				Fe(III) (wt%)				$Fe(III)/Fe_T$				LOI (wt%)			
Variable/Statistic	**mean**	**Std dev**	**median**	**n**	**mean**	**Std dev**	**median**	**n**	**mean**	**Std dev**	**median**	**n**	**mean**	**Std dev**	**median**	**n**
By published geologic setting																
alpine ophiolite	7.24	0.79	7.16	77	3.39	1.13	3.38	68	0.62	0.19	0.66	68	10.59	2.69	11.84	66
alpine peridotite	7.44	0.64	7.58	52	2.52	1.44	2.22	52	0.43	0.24	0.41	52	6.94	4.42	5.96	31
alpine serpentinite	7.17	0.88	7.20	25	2.87	1.18	3.43	25	0.52	0.21	0.61	25	10.41	4.58	11.97	25
forearc	6.62	0.42	6.62	17	2.18	0.82	2.02	7	0.43	0.16	0.42	7	14.84	1.16	15.13	14
MOR	7.11	1.34	6.90	163	3.48	1.33	3.51	169	0.61	0.18	0.62	180	12.19	2.90	12.73	158
MOR hydrothermal field	7.71	2.48	7.10	24	4.20	2.03	4.48	7	0.63	0.12	0.63	7	13.77	0.94	13.50	24
OCC	8.13	1.23	7.83	47	NA	NA	NA	0	NA	NA	NA	0	11.68	2.85	12.60	46
ophiolite	7.06	1.82	7.31	215	3.25	1.32	2.98	168	0.59	0.21	0.58	170	11.94	6.47	11.59	205
passive margin	6.47	0.59	6.48	56	2.74	0.50	2.75	46	0.54	0.08	0.55	46	16.19	1.40	16.10	52
By inferred initial setting/process																
accretionary wedge	7.40	1.23	7.21	73	2.91	1.33	2.76	73	0.51	0.21	0.53	73	10.33	4.45	11.62	73
forearc	6.62	0.42	6.62	17	2.18	0.82	2.02	7	0.43	0.16	0.42	7	14.84	1.16	15.13	14
fracture zone	6.46	0.37	6.44	17	2.65	0.50	2.79	17	0.52	0.09	0.55	17	13.60	1.80	14.03	17
mantle wedge	7.06	0.78	7.10	28	2.48	0.62	2.49	28	0.46	0.12	0.46	28	10.65	2.83	10.70	28
MOR OCC	7.44	1.57	7.20	214	3.59	1.40	3.60	156	0.62	0.18	0.63	167	12.18	2.81	12.83	208
passive margin	6.43	0.70	6.48	74	2.92	0.63	2.83	64	0.59	0.11	0.58	64	15.20	2.11	15.70	70
subduction zone	7.65	0.60	7.60	44	2.87	1.19	2.97	32	0.49	0.18	0.50	32	8.89	3.41	10.50	33
By rock type																
Amphibole-Gabbro	4.48	NA	4.48	1	0.90	NA	0.90	1	0.26	NA	0.26	1	2.77	NA	2.77	1
antigorite serpentinite	7.13	0.76	7.20	13	3.33	1.04	2.99	9	0.61	0.17	0.57	9	11.80	0.31	11.60	9
Atg Chl Opx Ol rock	7.51	0.78	7.16	5	2.97	0.00	2.97	3	0.52	0.02	0.53	3	10.01	0.24	10.01	2
Atg Liz serpentinite	7.42	0.61	7.10	5	3.26	0.74	3.00	5	0.58	0.08	0.60	5	11.32	0.30	11.30	5
carbonated serpentinite	3.91	2.37	4.10	17	NA	NA	NA	0	NA	NA	NA	0	28.80	2.23	27.51	17
chrysotile lizardite serpentinite	3.69	NA	3.69	1	2.61	NA	2.61	1	0.91	NA	0.91	1	13.65	NA	13.65	1
Diabase	8.38	NA	8.38	1	1.27	NA	1.27	1	0.19	NA	0.19	1	0.88	NA	0.88	1
dunite	10.97	NA	10.97	1	8.20	NA	8.20	1	0.96	NA	0.96	1	13.90	NA	13.90	1
granofels chl harz	7.93	0.21	8.00	3	2.29	0.42	2.29	2	0.38	0.05	0.38	2	4.96	0.78	4.96	2
Liz serpentinite	7.15	0.21	7.15	2	3.70	0.14	3.70	2	0.65	0.07	0.65	2	12.65	0.55	12.65	2
ol opx serpentinite	7.16	0.86	7.16	2	2.15	0.00	2.15	2	0.39	0.04	0.39	2	7.29	0.43	7.29	2
Ol2 Atg serpentinite	7.95	0.49	7.95	2	2.10	1.56	2.10	2	0.35	0.21	0.35	2	8.90	1.00	8.90	2
Olivine-Gabbro	8.82	0.97	8.82	2	2.48	1.24	2.48	2	0.38	0.22	0.38	2	5.52	4.75	5.52	2
peridotite	7.29	3.34	7.42	3	3.31	1.76	4.14	3	0.57	0.15	0.55	3	7.98	1.07	6.91	3
serpentinite	7.30	1.31	7.12	352	3.36	1.28	3.26	296	0.59	0.19	0.60	309	12.20	0.18	12.57	330
serpentinized dunite	7.72	1.21	7.59	71	3.45	1.46	3.56	54	0.57	0.18	0.62	54	11.29	0.43	12.00	71
serpentinized harzburgite	6.92	1.32	6.99	212	3.01	1.36	3.02	184	0.57	0.23	0.60	184	10.94	0.26	12.35	191
serpentinized lherzolite	8.74	1.27	8.79	14	4.37	0.69	4.65	14	0.65	0.08	0.62	14	10.89	0.57	11.41	14
serpentinized troctolite	10.20	0.69	10.22	6	NA	NA	NA	0	NA	NA	NA	0	4.68	0.63	4.73	5
serpentinized websterite	4.83	NA	4.83	1	NA	NA	NA	0	NA	NA	NA	0	13.33	NA	13.33	1
serpentinized wehrlite	9.16	0.16	9.16	2	6.55	0.16	6.55	2	0.92	0.01	0.92	2	10.81	0.08	10.81	2
spinifex like chl harz	7.72	0.48	7.60	5	2.41	0.28	2.41	3	0.40	0.04	0.41	3	5.71	0.90	5.71	2
talc chlorite serpentinite	10.41	NA	10.41	1	2.39	NA	2.39	1	0.29	NA	0.29	1	7.16	NA	7.16	1
By sample type																
core	6.94	1.21	6.79	213	2.96	1.00	2.99	178	0.55	0.14	0.58	187	13.08	0.24	13.59	200
dive	8.67	4.65	7.37	6	4.02	2.20	3.44	6	0.59	0.11	0.57	6	13.74	0.49	13.77	6
dredge	7.60	1.28	7.46	67	4.44	1.28	4.27	42	0.75	0.15	0.75	42	12.77	0.22	13.02	67
drill hole	7.16	0.82	7.16	15	3.55	0.64	3.63	15	0.64	0.11	0.66	15	13.54	0.50	13.50	15
grab	7.36	1.24	6.90	17	NA	NA	NA	0	NA	NA	NA	0	13.71	0.21	13.50	17
outcrop	7.05	1.64	7.36	237	2.81	1.20	2.71	184	0.51	0.22	0.50	186	11.22	0.49	10.47	195
By bulk rock method																
electron microprobe	8.09	1.62	7.48	5	-	-	-	-	-	-	-	-	-	-	-	-
ICP	9.47	1.20	9.73	11	-	-	-	-	-	-	-	-	-	-	-	-
ICP-AES	7.06	0.84	7.09	97	-	-	-	-	-	-	-	-	-	-	-	-
ICP-OES	7.80	2.12	7.44	48	-	-	-	-	-	-	-	-	-	-	-	-
unknown	7.52	1.29	7.30	235	-	-	-	-	-	-	-	-	-	-	-	-
wet chemistry	7.49	1.24	7.31	23	-	-	-	-	-	-	-	-	-	-	-	-
XRF	6.82	1.55	6.89	303	-	-	-	-	-	-	-	-	-	-	-	-
By Fe(II)/(III) method																
Mossbauer	-	-	-	-	3.08	1.02	3.45	10	0.54	0.16	0.61	10	NA	NA	NA	NA
wet chemistry	-	-	-	-	2.97	1.20	2.87	338	0.55	0.19	0.56	343	NA	NA	NA	NA

Table S3.

	FeO_T (wt%)				Fe(III) (wt%)				$Fe(III)/Fe_T$			
Variable/Statistic	**mean**	**Std dev**	**median**	**n**	**mean**	**Std dev**	**median**	**n**	**mean**	**Std dev**	**median**	**n**
By published geologic setting												
alpine ophiolite	4.12	0.36	4.24	11	2.03	0.43	2.01	5	0.66	0.18	0.64	22
alpine serpentinite	2.40	1.31	2.40	19	0.49	0.12	0.45	11	0.47	0.18	0.41	11
forearc	6.83	3.67	5.68	159	NA	NA	NA	0	NA	NA	NA	0
iron formation	1.10	NA	1.10	1	NA	NA	NA	0	NA	NA	NA	0
layered mafic intrusion	8.87	4.13	9.60	23	NA	NA	NA	0	NA	NA	NA	0
MOR	4.68	1.94	4.38	261	1.78	0.72	1.63	10	0.57	0.17	0.61	24
MOR hydrothermal field	1.69	NA	1.69	1	NA	NA	NA	0	NA	NA	NA	0
OCC	4.30	2.13	3.73	270	NA	NA	NA	0	NA	NA	NA	0
ophiolite	4.23	2.36	3.52	284	1.06	0.55	1.01	78	0.50	0.26	0.51	78
passive margin	4.97	2.33	4.72	161	0.63	NA	0.63	1	0.79	NA	0.79	1
serpentine mud volcano	6.06	2.35	5.64	39	NA	NA	NA	0	NA	NA	NA	0
sill	NA	NA	NA	0	0.41	0.57	0.41	2	0.44	0.62	0.44	2
By inferred initial setting/process												
accretionary wedge	3.70	1.98	3.35	45	0.73	0.40	0.68	28	0.39	0.18	0.36	28
forearc	6.83	3.67	5.68	159	NA	NA	NA	0	NA	NA	NA	0
forearc mantle wedge	6.06	2.35	5.64	39	NA	NA	NA	0	NA	NA	NA	0
layered mafic intrusion	6.74	4.14	5.10	13	NA	NA	NA	0	NA	NA	NA	0
mantle wedge	6.16	1.22	6.00	21	NA	NA	NA	0	NA	NA	NA	0
MOR	4.86	2.39	3.98	8	NA	NA	NA	0	NA	NA	NA	0
MOR OCC	4.48	2.04	4.11	524	1.78	0.72	1.63	10	0.57	0.17	0.61	24
passive margin	4.97	2.30	4.72	167	0.63	NA	0.63	1	0.79	NA	0.79	1
subduction zone	4.36	1.94	4.03	20	2.03	0.43	2.01	5	0.66	0.18	0.65	21
By rock type												
antigorite serpentinite	3.57	0.30	3.49	4	0.95	0.57	0.95	2	0.40	0.17	0.48	3
Atg Chl Opx Ol rock	4.33	0.12	4.24	7	2.20	0.24	2.18	4	0.67	0.07	0.66	4
Atg Liz serpentinite	NA	NA	NA	0	NA	NA	NA	0	0.81	0.09	0.84	7
carbonated serpentinite	4.40	1.87	4.29	18	NA	NA	NA	0	NA	NA	NA	0
Liz serpentinite	NA	NA	NA	0	NA	NA	NA	0	0.93	NA	0.93	1
ol opx serpentinite	4.07	NA	4.07	1	NA	NA	NA	0	NA	NA	NA	0
Ol2 Atg serpentinite	NA	NA	NA	0	NA	NA	NA	0	0.54	0.13	0.54	2
olivine websterite	9.77	0.59	9.77	2	NA	NA	NA	0	NA	NA	NA	0
peridotite	4.40	0.42	4.40	2	NA	NA	NA	0	NA	NA	NA	0
serpentinite	4.94	2.51	5.05	237	0.68	0.47	0.48	50	0.41	0.26	0.38	62
serpentinized dunite	4.45	2.77	4.30	147	0.51	0.44	0.71	3	0.40	0.44	0.34	3
serpentinized harzburgite	4.87	2.68	4.34	778	1.21	0.63	1.07	67	0.56	0.24	0.61	72
serpentinized lherzolite	7.97	3.52	8.00	8	NA	NA	NA	0	NA	NA	NA	0
serpentinized troctolite	5.94	4.02	4.10	3	NA	NA	NA	0	NA	NA	NA	0
serpentinized websterite	5.47	3.57	4.53	31	NA	NA	NA	0	NA	NA	NA	0
serpentinized wehrlite	3.09	0.46	3.10	14	NA	NA	NA	0	NA	NA	NA	0
By sample type												
core	5.20	2.71	4.79	698	1.41	0.39	1.37	6	0.58	0.19	0.57	18
dredge	4.21	2.04	3.56	151	2.34	0.79	2.54	4	0.51	0.17	0.53	4
drill cuttings	7.46	0.66	7.46	2	NA	NA	NA	0	NA	NA	NA	0
drill hole	1.55	0.80	1.28	11	0.49	0.12	0.45	11	0.47	0.18	0.41	11
grab	1.69	NA	1.69	1	NA	NA	NA	0	NA	NA	NA	0
mud cores	6.06	2.35	5.64	39	NA	NA	NA	0	NA	NA	NA	0
outcrop	4.23	2.23	3.67	176	1.05	0.65	1.03	83	0.49	0.29	0.50	86
By mineral chemistry method												
EDS	4.87	1.24	4.65	6	-	-	-	-	-	-	-	-
electron microprobe	4.87	2.66	4.46	1231	-	-	-	-	-	-	-	-
unknown	2.64	3.76	1.53	13	-	-	-	-	-	-	-	-
By Fe(II)/(III) method												
Mossbauer	-	-	-	-	0.96	0.57	0.92	91	0.47	0.29	0.41	86
uXANES	-	-	-	-	2.20	0.24	2.18	4	0.60	0.20	0.61	43

A

F = 33.138 on 4/322 d.f.

p = 0

serpentinized harzburgite
n = 212
AB

serpentinized dunite
n = 71
B

carbonated serpentinite
n = 17
A

serpentinized lherzolite
n = 14
B

antigorite serpentinite
n = 13
B

D

F = 5.389 on 3/257 d.f.

p = 0.00162

serpentinized harzburgite
n = 184
A

serpentinized dunite
n = 54
A

serpentinized lherzolite
n = 14
A

antigorite serpentinite
n = 9
A

G

F = 0.71 on 3/257 d.f.

p = 0.55

serpentinized harzburgite
n = 184

serpentinized dunite
n = 54

serpentinized lherzolite
n = 14

antigorite serpentinite
n = 9

B

F = 2.975 on 4/544 d.f.

p = 0.0199

outcrop
n = 237

core
n = 213

dredge
n = 67

grab
n = 17

drill hole
n = 15

E

F = 26.139 on 3/415 d.f.

p = 0

outcrop
n = 184
A

core
n = 178
AB

dredge
n = 42
C

drill hole
n = 15
B

H

F = 20.725 on 3/426 d.f.

p = 0

core
n = 187
AB

outcrop
n = 186
A

dredge
n = 42
C

drill hole
n = 15
B

Frequency

C

F = 12.703 on 4/477 d.f.

p = 0

XRF
n = 303
AB

ICP−AES
n = 97
A

ICP−OES
n = 48
AB

wet chemistry
n = 23
B

ICP
n = 11
C

0 2 4 6 8 10 12 14 16 18

FeO_T wt%

F

F = 0.085 on 1/346 d.f.

p = 0.766

wet chemistry
n = 338

mossbauer
n = 10

0 1 2 3 4 5 6 7 8 9

FeIII wt%

I

F = 0.04 on 1/351 d.f.

p = 0.848

wet chemistry
n = 343

mossbauer
n = 10

0.0 0.2 0.4 0.6 0.8 1.0

$FeIII/Fe_T$

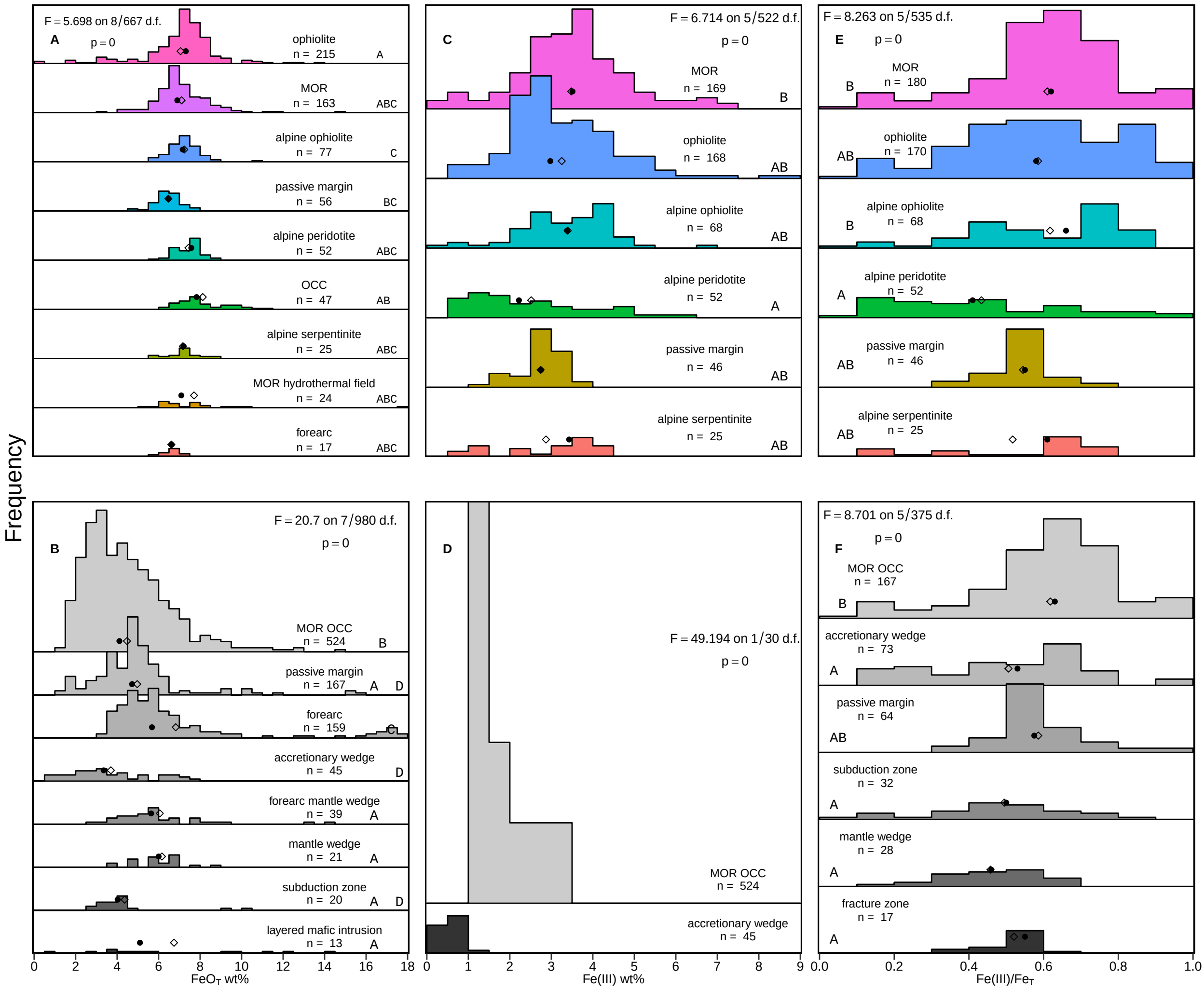
A
F = 5.698 on 8/667 d.f.
p = 0
ophiolite
n = 215
A
MOR
n = 163
ABC
alpine ophiolite
n = 77
C
passive margin
n = 56
BC
alpine peridotite
n = 52
ABC
OCC
n = 47
AB
alpine serpentinite
n = 25
ABC
MOR hydrothermal field
n = 24
ABC
forearc
n = 17
ABC
C
F = 6.714 on 5/522 d.f.
p = 0
MOR
n = 169
B
ophiolite
n = 168
AB
alpine ophiolite
n = 68
AB
alpine peridotite
n = 52
A
passive margin
n = 46
AB
alpine serpentinite
n = 25
AB
E
F = 8.263 on 5/535 d.f.
p = 0
MOR
n = 180
B
ophiolite
n = 170
AB
alpine ophiolite
n = 68
B
alpine peridotite
n = 52
A
passive margin
n = 46
AB
alpine serpentinite
n = 25
AB
Frequency
B
F = 20.7 on 7/980 d.f.
p = 0
MOR OCC
n = 524
B
passive margin
n = 167
A D
forearc
n = 159
C
accretionary wedge
n = 45
D
forearc mantle wedge
n = 39
A
mantle wedge
n = 21
A
subduction zone
n = 20
A D
layered mafic intrusion
n = 13
A
0 2 4 6 8 10 12 14 16 18
FeO$_T$ wt%
D
F = 49.194 on 1/30 d.f.
p = 0
MOR OCC
n = 524
accretionary wedge
n = 45
0 1 2 3 4 5 6 7 8 9
Fe(III) wt%
F
F = 8.701 on 5/375 d.f.
p = 0
MOR OCC
n = 167
B
accretionary wedge
n = 73
A
passive margin
n = 64
AB
subduction zone
n = 32
A
mantle wedge
n = 28
A
fracture zone
n = 17
A
0.0 0.2 0.4 0.6 0.8 1.0
Fe(III)/Fe$_T$

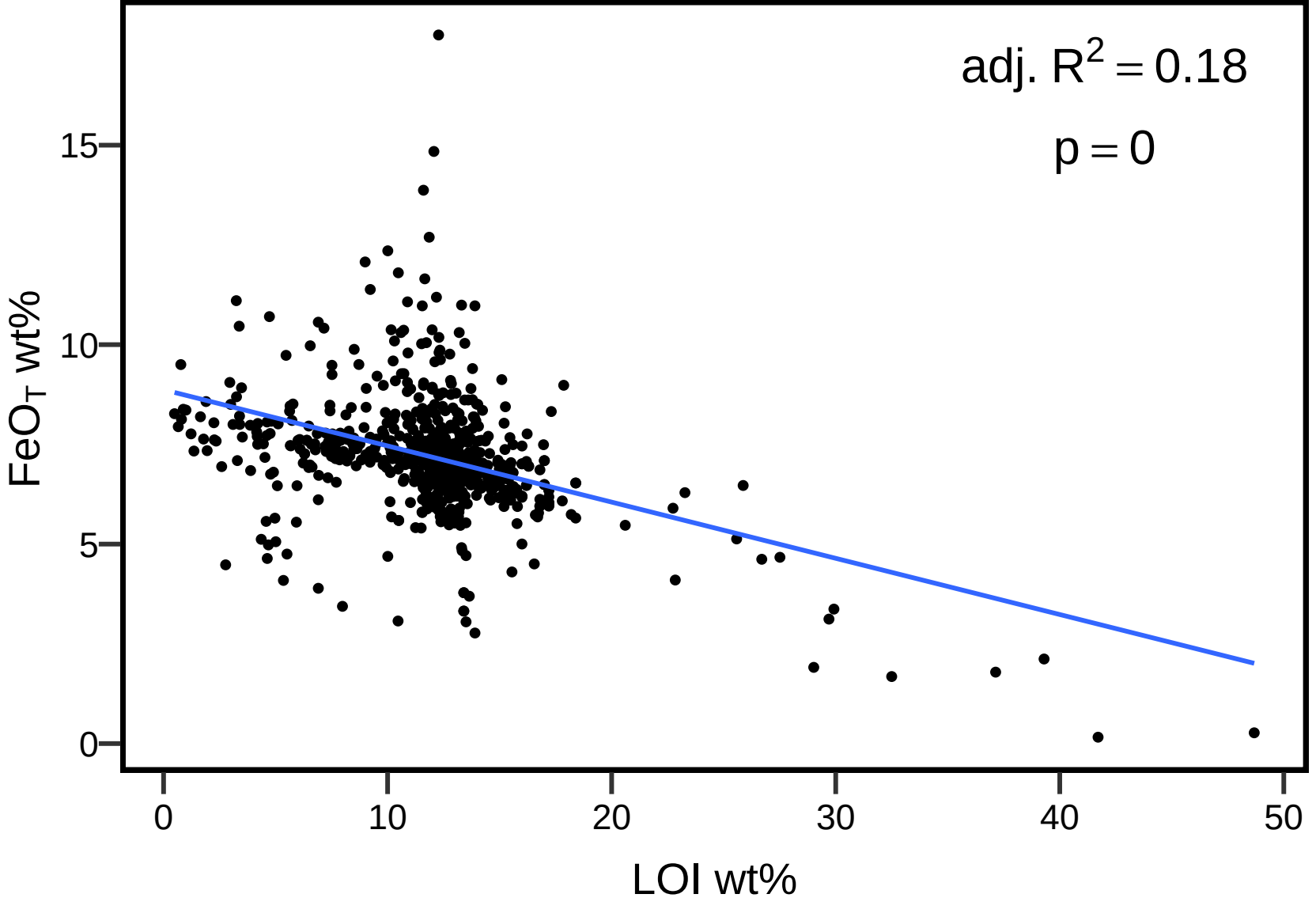
adj. $R^2 = 0.18$
$p = 0$
15
10
5
0
FeO_T wt%
0
10
20
30
40
50
LOI wt%

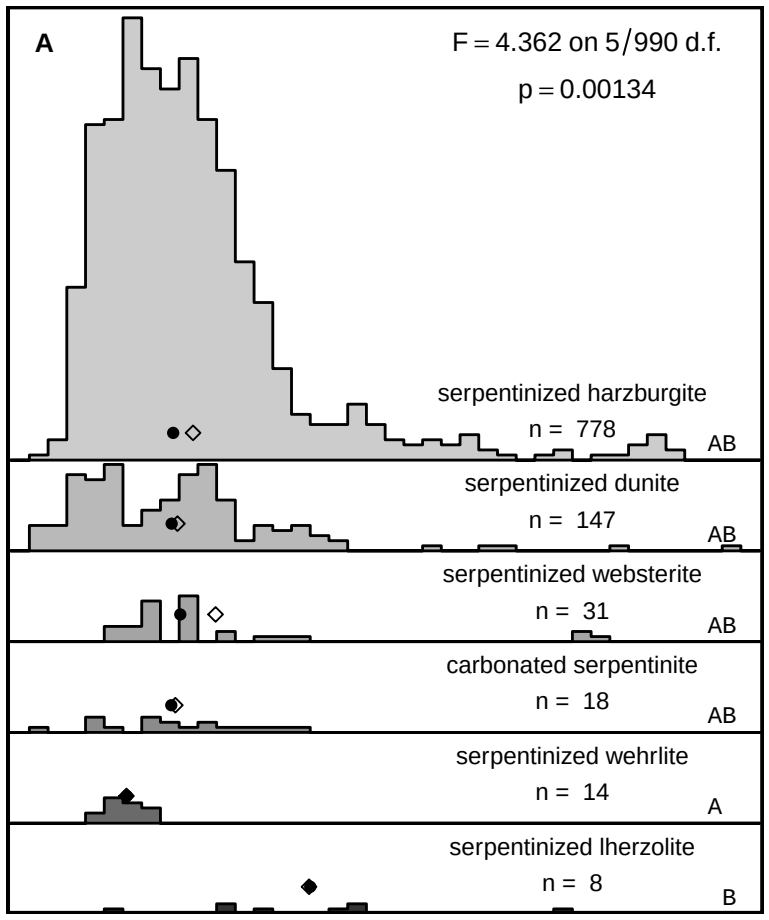
A
F = 4.362 on 5/990 d.f.
p = 0.00134
serpentinized harzburgite
n = 778
AB
serpentinized dunite
n = 147
AB
serpentinized websterite
n = 31
AB
carbonated serpentinite
n = 18
AB
serpentinized wehrlite
n = 14
A
serpentinized lherzolite
n = 8
B

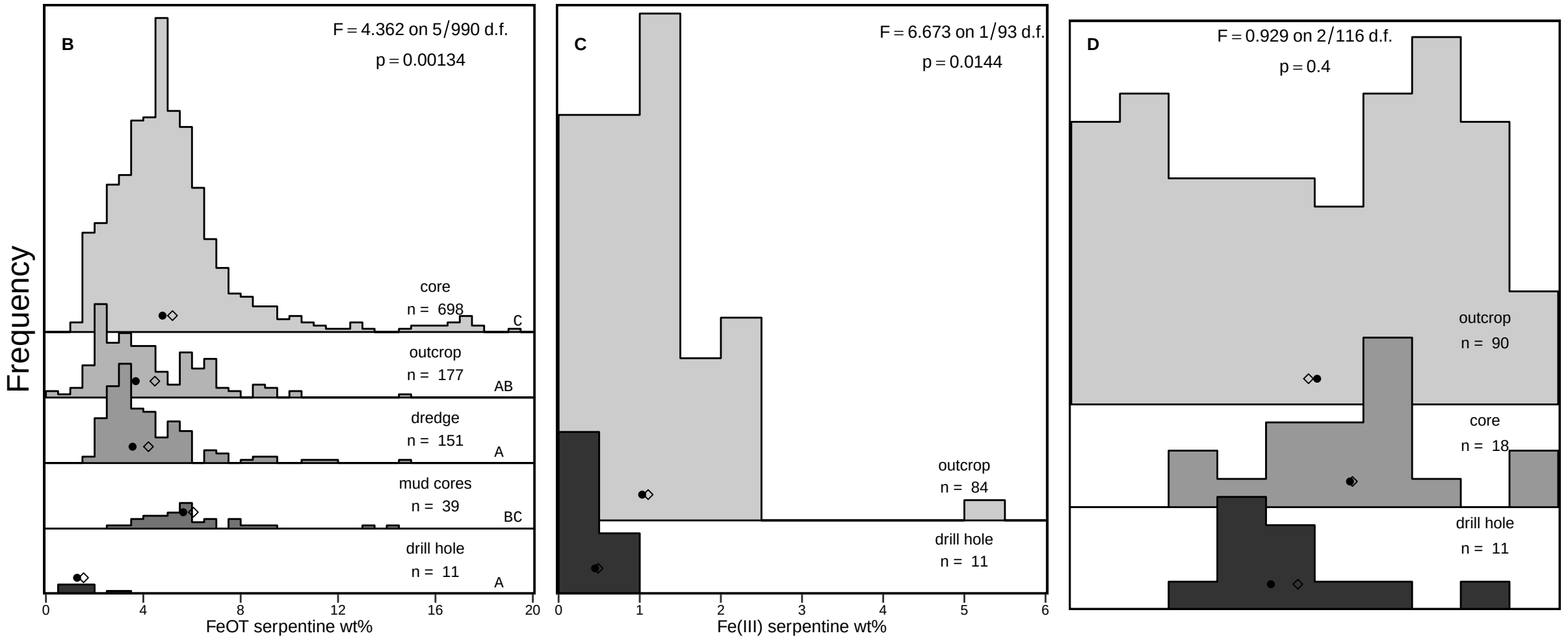
Frequency
B
F = 4.362 on 5/990 d.f.
p = 0.00134
core
n = 698
C
outcrop
n = 177
AB
dredge
n = 151
A
mud cores
n = 39
BC
drill hole
n = 11
A
0
4
8
12
16
20
FeOT serpentine wt%
C
F = 6.673 on 1/93 d.f.
p = 0.0144
outcrop
n = 84
drill hole
n = 11
0
1
2
3
4
5
6
Fe(III) serpentine wt%
D
F = 0.929 on 2/116 d.f.
p = 0.4
outcrop
n = 90
core
n = 18
drill hole
n = 11

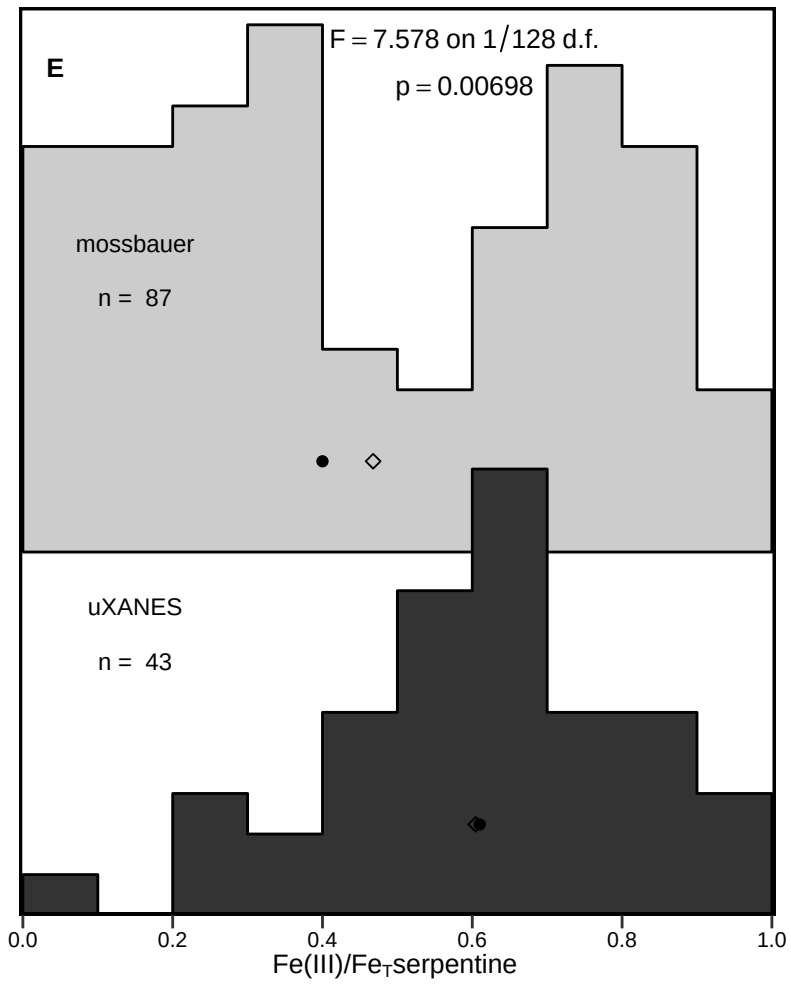
E
F = 7.578 on 1/128 d.f.
p = 0.00698
mossbauer
n = 87
uXANES
n = 43
0.0
0.2
0.4
0.6
0.8
1.0
Fe(III)/Fe$_T$serpentine

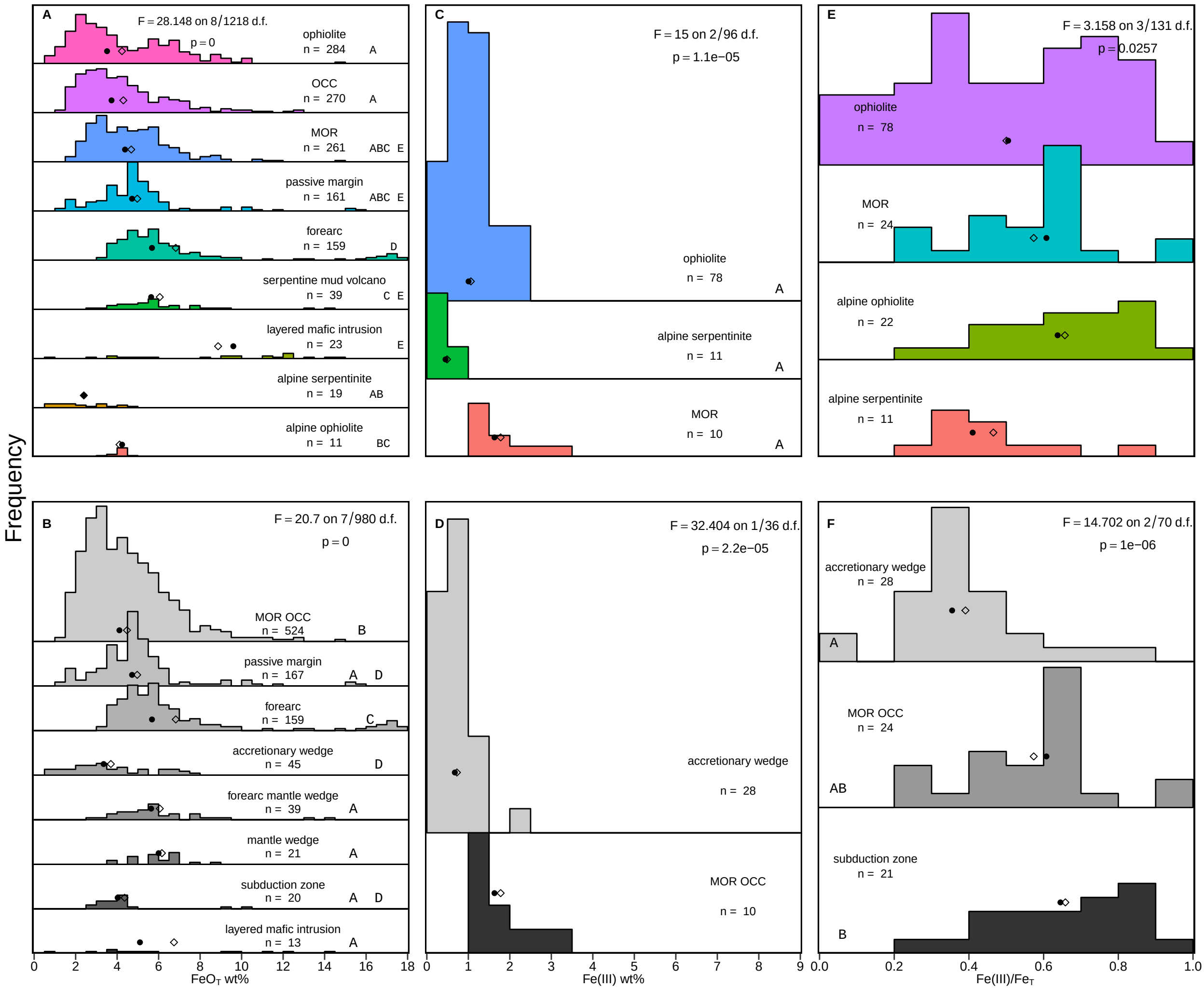
A
F = 28.148 on 8/1218 d.f.
p = 0
ophiolite
n = 284
A
OCC
n = 270
A
MOR
n = 261
ABC E
passive margin
n = 161
ABC E
forearc
n = 159
D
serpentine mud volcano
n = 39
C E
layered mafic intrusion
n = 23
E
alpine serpentinite
n = 19
AB
alpine ophiolite
n = 11
BC
C
F = 15 on 2/96 d.f.
p = 1.1e−05
ophiolite
n = 78
A
alpine serpentinite
n = 11
A
MOR
n = 10
A
E
F = 3.158 on 3/131 d.f.
p = 0.0257
ophiolite
n = 78
MOR
n = 24
alpine ophiolite
n = 22
alpine serpentinite
n = 11
Frequency
B
F = 20.7 on 7/980 d.f.
p = 0
MOR OCC
n = 524
B
passive margin
n = 167
A D
forearc
n = 159
C
accretionary wedge
n = 45
D
forearc mantle wedge
n = 39
A
mantle wedge
n = 21
A
subduction zone
n = 20
A D
layered mafic intrusion
n = 13
A
0 2 4 6 8 10 12 14 16 18
FeO$_T$ wt%
D
F = 32.404 on 1/36 d.f.
p = 2.2e−05
accretionary wedge
n = 28
MOR OCC
n = 10
0 1 2 3 4 5 6 7 8 9
Fe(III) wt%
F
F = 14.702 on 2/70 d.f.
p = 1e−06
accretionary wedge
n = 28
A
MOR OCC
n = 24
AB
subduction zone
n = 21
B
0.0 0.2 0.4 0.6 0.8 1.0
Fe(III)/Fe$_T$

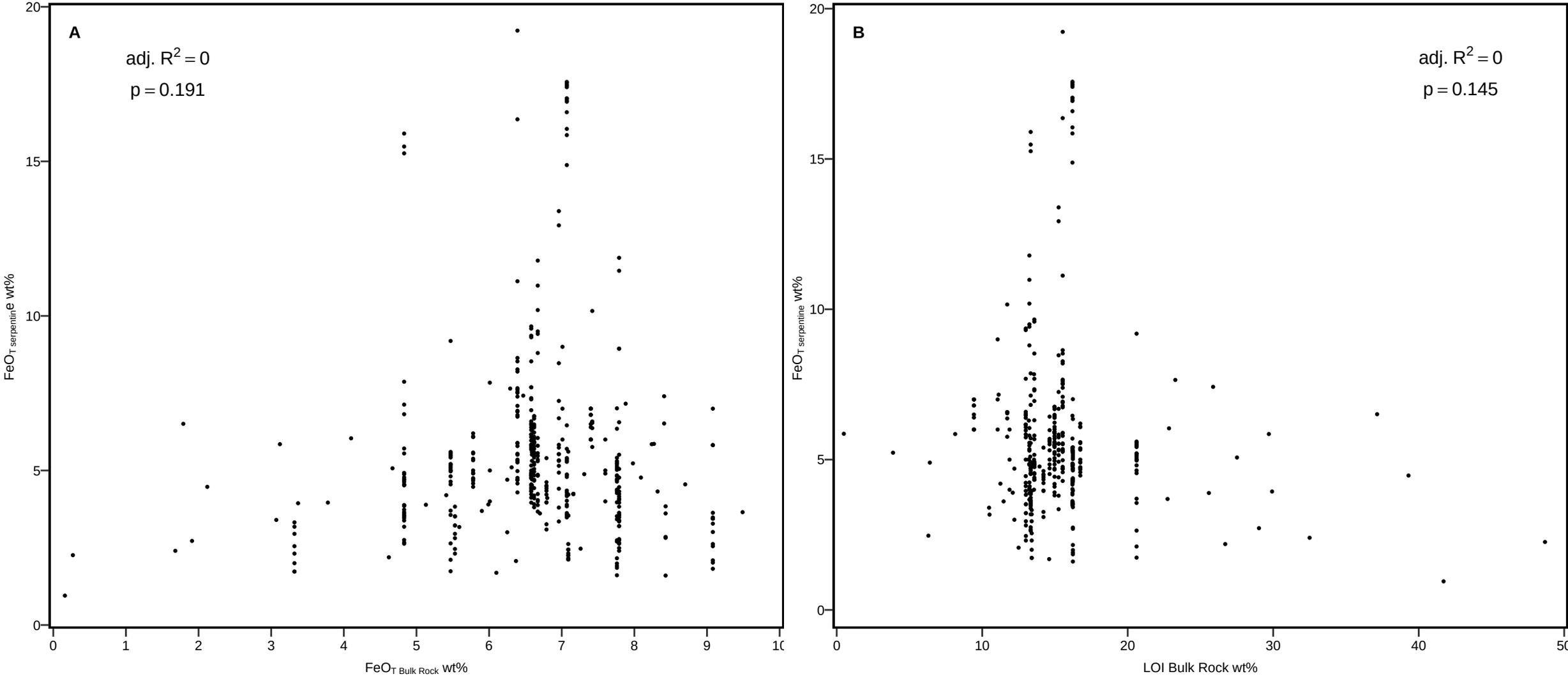
A
adj. $R^2 = 0$
$p = 0.191$
$FeO_{T\ serpentine}$ wt%
$FeO_{T\ Bulk\ Rock}$ wt%
0
5
10
15
20
0
1
2
3
4
5
6
7
8
9
10

B
adj. $R^2 = 0$
$p = 0.145$
$FeO_{T\ serpentine}$ wt%
LOI Bulk Rock wt%
0
5
10
15
20
0
10
20
30
40
50